Materials Science in Semiconductor Processing 31 (2015) 372–379

Contents lists available at ScienceDirect

Materials Science in Semiconductor Processing

journal homepage: www.elsevier.com/locate/mssp

Electronic structure, chemical bonding and optical properties of Di-2-pyrymidonium dichloride diiodide ($C_4H_5ClIN_2O$) from first-principles

Sikander Azam [a], A.H. Reshak [a,b,*]

[a] New Technologies – Research Center, University of West Bohemia, Univerzitni 8, 306 14 Pilsen, Czech Republic
[b] Center of Excellence Geopolymer and Green Technology, School of Material Engineering, Universiti Malaysia Perlis, 01007 Kangar, Perlis, Malaysia

ARTICLE INFO

Keywords:
Electronic structure
Electronic charge density
Optical properties

ABSTRACT

The electronic structure and electronic charge density of the monoclinic phase Di-2-pyrymidonium dichloride-di-iodide compound is studied by using the local density approximation (LDA) and Engel Vosko generalized gradient approximation (EVGGA). Using LDA for exchange correlation potential, we have optimized the atomic positions taken from the X-ray crystallographic data by minimization of the forces acting on the atoms. From the relaxed geometry the electronic structure, electronic charge density and the optical properties were determined. Band structures disclose that this compound has indirect energy band gap. The obtained energy band gap value using EVGGA (2.010 eV) is larger than that obtained within LDA (1.781 eV). To envision the chemical bonding nature between the composition of the investigated compound, the distribution of charge density was discussed in the (−1 0 1) crystallographic plane. The contour plot shows partial ionic and strong covalent bonding between C–O, N–C and C–H atoms. The optical properties of Di-2-pyrymidonium dichloride-di-iodide are obtained by the calculation of the dielectric function.

1. Introduction

The organic iodine materials are very promising for the photoinduced nonlinear optics [1] which may stimulate additional interest to such kind of semi-conducting materials. Recently the importance of iodine chemistry is being proved by the discovery of semi- and superconducting polyiodides and low temperature, quickly leading to the deliberate doping of conjugated polymers along with the elemental iodine [2]. The iodine has the potential to catenate the configuration of polyiodides possessing various structures, as studied recently by Deplano et al., Svensson et al. and Boyle et al. [2–5].

The reaction of diiodine with heterocycles (ketones, thiones or selones) results in different natures of iodine compounds, like charge transfer complexes, with "extended spoke structures" (D–I_2–I_2), "spoke structures" (D–I_2; D=donor), iodonium salts, monocationic disulfides and dicationic disulfides or diselenides [6]. Contingent on the conductivity measurements, Parigoridi et al. [6] studied that the equilibrium is established between "spoke" and an iodonium structure in solution in the reaction of thioamides and I_2. In 2004, Barluenga et al. [7] investigated the catalytic activity on alcohol oxidation by the iodonium salt of formula $[I(Py)_2][BF_4]$ (Py=pyridine), also other substituted organic iodine (iodine(V), [8] iodine(III) [9] or iodine(I) [10,11]) compounds were tried.

In 2008, Parigoridi et al. [6] studied the interaction of thioamides with diiodine, synthesized and crystallographically characterized the ionic $([C_4H_5N_2O]^+)_2[I_2Cl_2]^{2-}$ complex holding the $[I_2Cl_2]^{2-}$ anion, which were observed for

* Corresponding author. Tel.: +420 777729583.
E-mail address: maalidph@yahoo.co.uk (A.H. Reshak).

http://dx.doi.org/10.1016/j.mssp.2014.12.009
1369-8001/

the first time and the $[(tzdtH)I_2]_2 \cdot I_2$ (2a) (tzdtH=thiazolidine-2-thione), which achieved a co-product of the $[(tzdtH)_2I]^+[I_3]^- \cdot 2I_2$ (2) complex. To the best of our knowledge, no theoretical work on electronic structure and optical properties on Di-2-pyrymidonium dichloride-di-iodide ($C_4H_5ClIN_2O$) has been reported in literature. Therefore, it inspires us to deal with the electronic structure and optical properties of Di-2-pyrymidonium dichloride-di-iodide ($C_4H_5ClIN_2O$) in the present paper. So in this work, the full-potential linearized augmented plane-wave (FPLAPW) method based on the first-principles density functional theory (DFT) within the local density approximation (LDA) and Engel–Vosko generalized gradient approximation (EVGGA) exchange potential approximation are used to calculate accurately the electronic band structure and optical properties of the Di-2-pyrymidonium dichloride-di-iodide.

The rest of the paper has been divided into three parts. In Section 2, we briefly describe the computational method used in this study. The most relevant results obtained for the electronic and optical properties of $C_4H_5ClIN_2O$ are presented and discussed in Section 3. Finally, we summarize the main conclusions in Section 4.

2. Computational details

We have used the crystallographic data (CCDC 679938) of Di-2-pyrymidonium dichloride-di-iodide, obtained from Cambridge Crystallographic database. The investigated compound crystallizes in monoclinic symmetry [6]. The molecular and unit cell crystal structure of Di-2-pyrymidonium dichloride-di-iodide has been shown in Fig. 1. We have performed first principle calculations based on the all-electron full-potential linearized augmented plane-wave (FPLAPW) method to solve the Kohn Sham DFT equations within the framework of the WIEN2K code [12]. This is an implementation of the DFT [13,14] with different possible approximations for the exchange correlation (XC) potentials. Exchange and correlation potential is described by the local density approximation (LDA) by Ceperley–Alder (CA) [15]. In addition, the Engel–Vosko generalized gradient approximation (EV-GGA) [16] was employed. As it is well known that LDA and GGA approaches have simple forms that are not sufficiently flexible to accurately reproduce both the exchange-correlation energy and its charge derivative. Engel and Vosko considered this shortcoming and constructed a new functional form of GGA that is able to better reproduce the exchange potential at the expense of less agreement in the exchange energy. This approach, called EV-GGA, yields better band splitting and some other properties that mainly depend on the accuracy of the exchange-correlation potential [17–30]. The potential and charge density in the muffin-tin (MT) spheres are expanded in spherical harmonics with $l_{max}=8$. In the interstitial region the potential and the charge density are represented by Fourier series. Using LDA–CA exchange correlation potential, we have optimized the atomic positions taken from the crystallographic data by minimization of the forces acting on the atoms. From the relaxed geometry of the electronic structure, electronic charge density and the optical properties were determined. In Table 1, we have listed the optimized

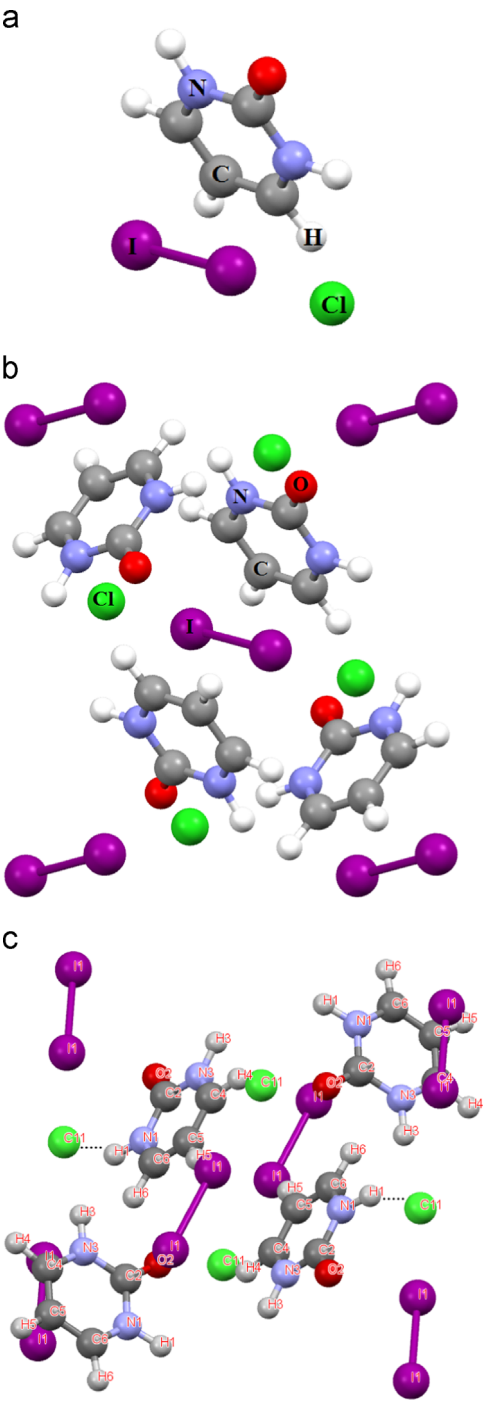

Fig. 1. Molecular, unit cell structure and hydrogen bonding of Di-2-pyrymidonium dichloride-di-iodide.

geometry along with the experimental one [6]. We have used 35 **k**-points in the irreducible Brillouin zone for structural optimization. For the calculation of electronic properties 300 **k**-points were used. The convergence of the self-consistent calculations is taken with respect to the total charge of the system with a tolerance of 0.0001 electrons.

3. Results and discussions

3.1. Electronic structure and charge density

The self-consistent full relativistic band structures calculations of the monoclinic phase Di-2-pyrymidonium dichloride-di-iodide compound were performed within LDA and EV-GGA schemes. The calculated band structure, obtained from the two types of exchange correlation is similar except the values of the band gap which is higher within EV-GGA. Fig. 2 illustrates the electronic band dispersion curves along high symmetry directions of the Brillion zone calculated for the equilibrium geometries of Di-2-pyrymidonium dichloride-di-iodide compound within the LDA and EV-GGA approximations. The top of the valence band maximum (VBM) occurs at D point and bottom of the conduction band minimum (CBM) occurs at r point resulting in an indirect energy band gap. The calculated band gaps are 1.781 (LDA) and 2.010 (EVGGA). As we have fixed E_F and also the VBM at $E=0$ eV, thus, the shifting of bands is expected only in CB in all formalisms. It is observed that the EV-GGA approximation formulates better band splitting. Thus, the VB and CB shift downwards and upwards, in energy as compared to energy bands in LDA, such that the difference between CB

Table 1
Atomic positions.

Atoms	Exp. X	Opt. X	Exp. Y	Opt. Y	Exp. Z	Opt. Z
N1	0.5367(6)	0.5345	0.1850(5)	0.1846	0.3248(5)	0.3217
H2	0.4708	0.4661	0.1225	0.1008	0.2878	0.2809
C3	0.6781(9)	0.6767	0.2162(6)	0.2160	0.2657(7)	0.2614
O4	0.7141(8)	0.7111	0.1597(5)	0.1600	0.1655(6)	0.1588
N5	0.7730(7)	0.7751	0.3169(5)	0.3178	0.3340(6)	0.3315
H6	0.8638	0.8874	0.3410	0.3443	0.3043	0.2949
C7	0.7332(9)	0.7371	0.3798(7)	0.3813	0.4435(7)	0.4431
H8	0.8022	0.8238	0.4484	0.4603	0.4837	0.4873
C9	0.5954(10)	0.5942	0.3459(7)	0.3474	0.4967(7)	0.4980
H10	0.5680	0.5638	0.3896	0.3969	0.5736	0.5898
C11	0.4977(9)	0.4934	0.2464(7)	0.2455	0.4352(8)	0.4333
H12	0.4019	0.3796	0.2205	0.2102	0.4706	0.4702
I13	0.61675(5)	0.6191	0.52274(4)	0.5238	0.91617(5)	0.9146
Cl14	0.8810(2)	0.8759	0.58455(17)	0.5851	0.73236(18)	0.7333

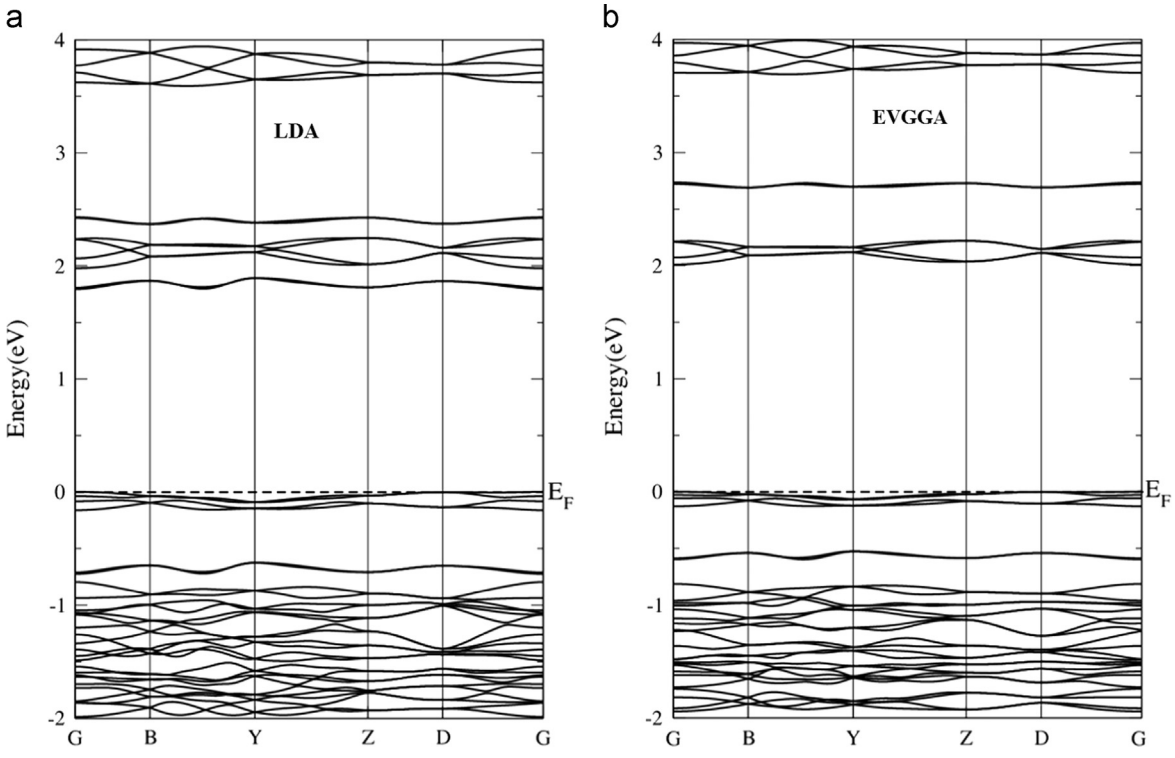

Fig. 2. Calculated band structure of Di-2-pyrymidonium dichloride-di-iodide.

minimum and VB maximum increases. We will discuss the rest of the results, obtained by the EVGGA functional, because this approach, yields better band splitting and some other properties.

In order to elucidate the nature of the electronic band structures, we have calculated the total and the partial densities of states (TDOS and PDOS) for the monoclinic phase of Di-2-pyrymidonium dichloride-di-iodide compound (Fig. 3). Following Fig. 3, we should highlight that there are four distinct structures separated by gaps. The first structure encountered in the TDOS, starting from −10.0 to −5.0 eV, consists of N-p, C-s, H-s, O-s and Cl-s orbitals. The next structure, lying between −5.0 eV and −2.4 eV is due to N-p, C-s, H-s, O-s and Cl-s orbitals. The third structure from −2.5 up to the Fermi level is due to Cl-p, I-p, and O-p states with small contribution from Cs-s and I-s states. Finally the last structure from 2.0 to 20.0 eV consists of I-p/d, N-p/d and C-s states. The PDOS show that there exists weak/strong hybridization. At the energy range between −10.00 and −4 eV there is a strong hybridization between N-s and Cl-s orbitals, H-s and O-s orbitals and N-p and C-s states. A strong hybridization between I-p and Cl-p appears at −3.0 eV and in the conduction bands.

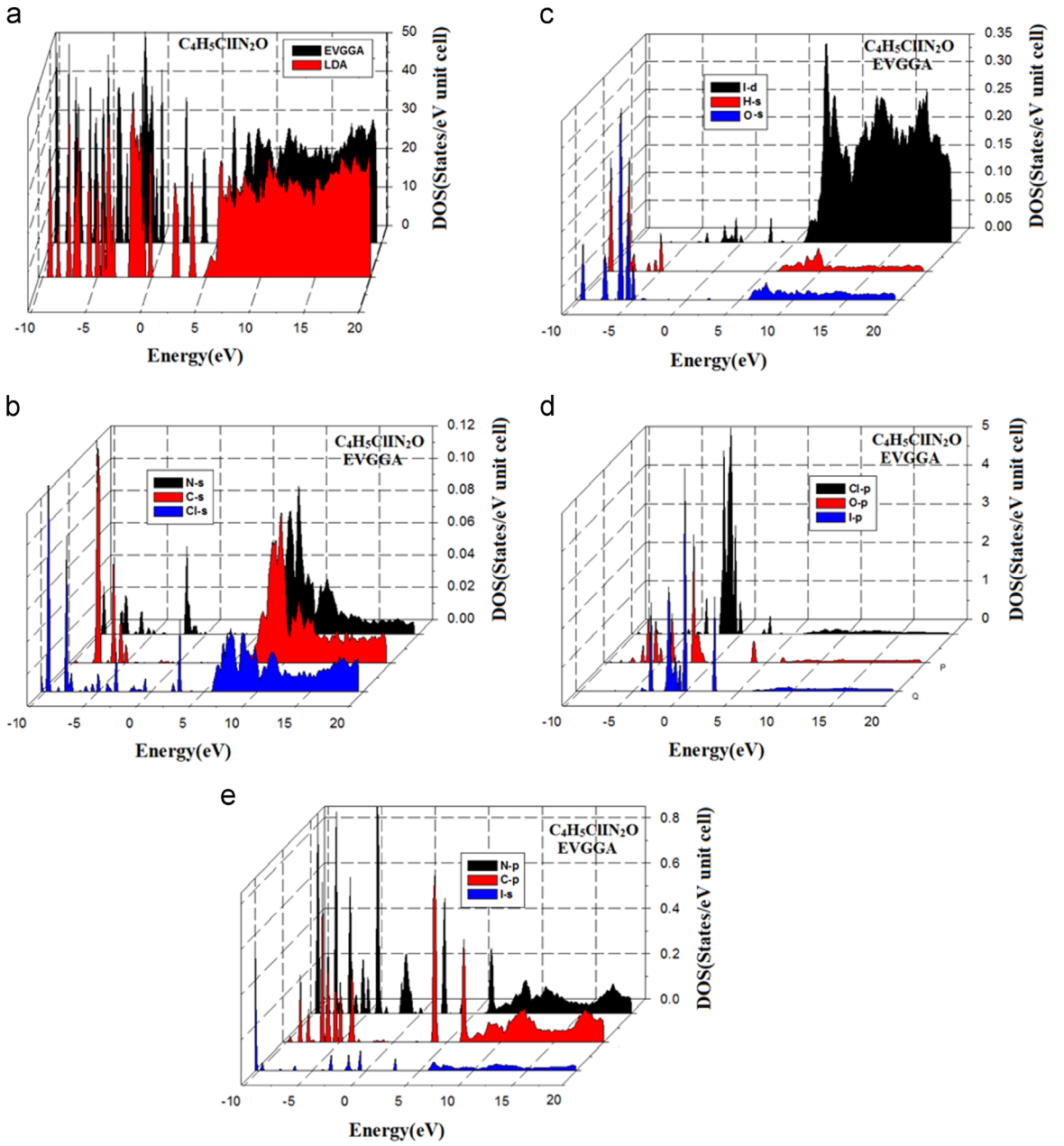

Fig. 3. Calculated total and partial densities of states (states/eV unit cell).

3.2. Electronic charge density

To envision the chemical bonding nature between the composition of Di-2-pyrymidonium dichloride-di-iodide, we have calculated the distribution of charge density in the (−1 01) crystallographic plane as shown in Fig. 4a. The contour plot shows partial ionic and strong covalent bonding between C–O, N–C and C–H atoms depending on Pauling electro-negativity difference of C (2.550), H (2.200) N (3.040), and O (3.44) atoms. From the electronic charge

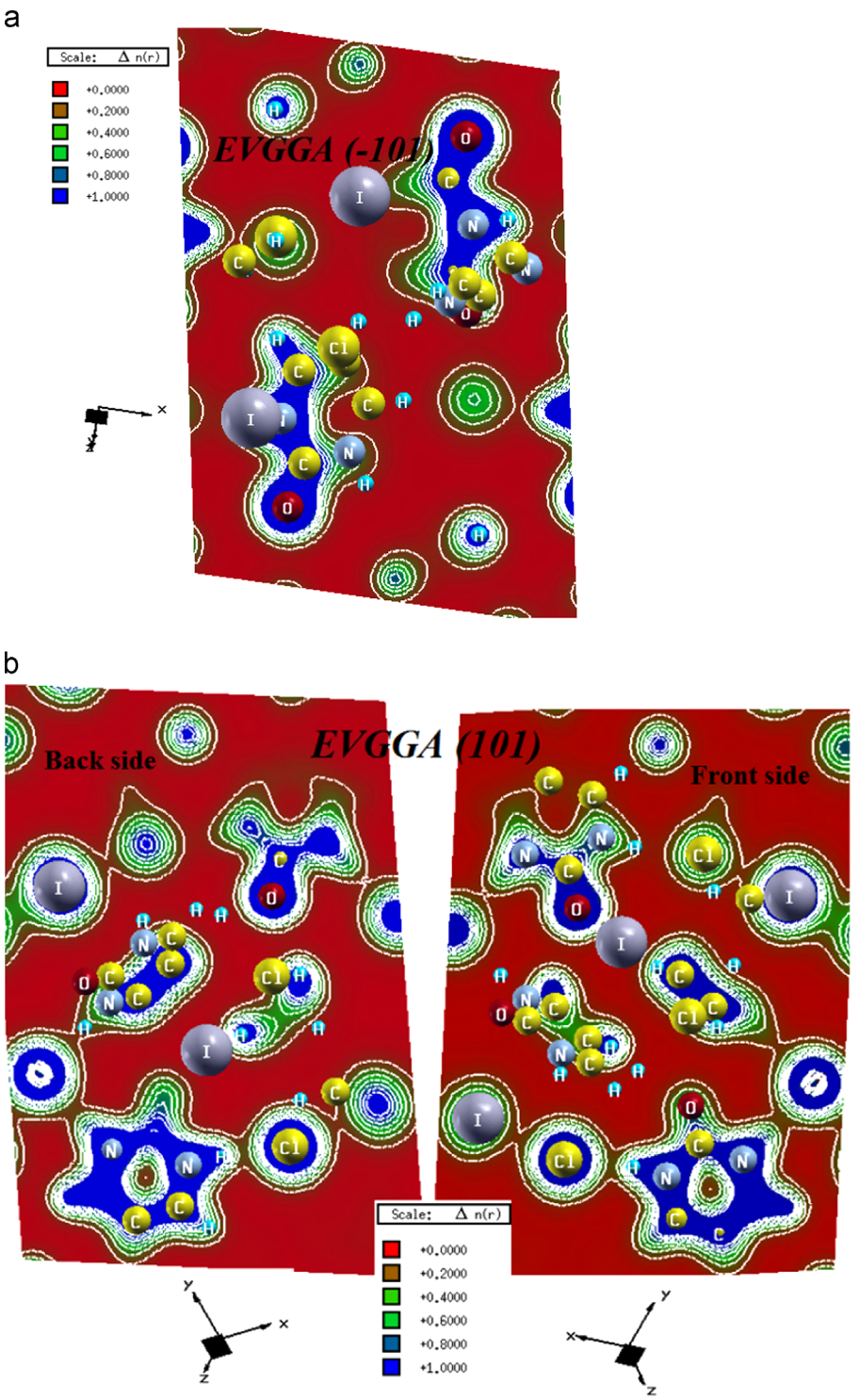

Fig. 4. Electronic charge density contour in the (−1 0 1) plane (a) LDA, (b) GGA, and (c) EV-GGA. (For interpretation of the references to color in this figure, the reader is referred to the web version of this article).

density plot it is clear that the majority of C, H, and N electronic charge is transferred to O atom. This is clear from the color charge density scale where blue color (+1.0000) communicates to the maximum charge accruing site. We also plotted the electron charge density contour in the (1 0 1) plane to discuss the anisotropy between the two planes in the crystal. To get full information about the electronic charge density of each atom we have plotted the front and back face of (1 0 1) plane (see Fig. 4b). Following two contour plots in the (−1 0 1) and (1 0 1) planes one can see that this crystal possesses a strong anisotropy which largesse to enhance the optical susceptibilities. As is clear from the charge density contour I atom does not appear in the (−1 0 1) plane, while it appears in the (1 0 1) plane presenting the ionic bond nature. Also in the (1 0 1) plane N–N, I–Cl and H–H making the covalent bonding, these bonds do not appear in the (−1 0 1) plane. In the (−1 0 1) plane the hydrogen has the ionic bond which does not appear in the (1 0 1) plane. The charge density along C–C, C–O, N–C and C–H bonds is pronounced. This is due to the strong hybridization of covalent C–O, C–C, C–H and C–N bonds. We should emphasize that the charge density distribution is essentially spherical around all the atoms. The O atom is more electronegative than C, H and S atoms, as one can clearly see that the charge accumulates more near O along the bonds and the charge around O is uniformly distributed. We also calculated the bond lengths and the bond angles which show good agreement with the experimental work [6] in Tables 2 and 3. The I1–I1–Cl is 177.9 bond angle which is linear. The extended inter-molecular hydrogen bonding (N–H···Cl) interaction has also been observed in Fig. 1(c).

Table 2
Bond lengths.

Atoms	Exp.	Opt.	Atoms	Exp.	Opt.
N3–C4	1.339(10)	1.345	I1–I1a	2.72(1)	2.783
C5–C6	1.360(11)	1.389	I1–Cl1	3.065	3.066
N1–C2	1.385(9)	1.402	C2–N3	1.373	1.397
N1–C6	1.327(9)	1.342	C2–O2	1.204(8)	1.223
C4–C5	1.337(11)	1.384			

Table 3
Bond angles.

Atom1	Exp.	Opt.
I1a–I1–Cl1	177.8(1)	177.9
O2–C2–N1	124.4(7)	123.5
O2–C2–N3	123.8(6)	123.6
C2–N1–C6	124.6(6)	124.5
C2–N3–C4	124.7(7)	124.1
N1–C2–N3	111.8(6)	112.8

3.3. Optical properties

In order to go deep in sight the electronic structures it is essential to investigate the optical spectra, which not only give information about the occupied and unoccupied states, but also about the features of the bands [31,32]. Optical spectroscopy analysis is a powerful tool for determining the overall band behavior of a solid [33]. The linear optical properties in solids are described by the dielectric tensor, the inter-band contribution to the imaginary part of its elements is calculated by summing transitions from occupied to unoccupied states over BZ, weighted with the appropriate

$$\mathrm{Im}\,\varepsilon_{\alpha\beta}(\omega)=\frac{4\pi^2e^2}{m^2\omega^2}\sum_{i,f}\int_{BZ}\frac{2dk}{2\pi^3}|\langle\phi_{fk}|P_\beta||\phi_{ik}\rangle\delta(E_f(k))-E_i(k)-\hbar\omega \quad (1)$$

and $\varepsilon_1(\omega)$ is the real part, which can be derived from the imaginary part by means of the Kramers–Kronig relation

$$\varepsilon_1(\omega)=1+\frac{2}{\pi}P\int_0^\infty\frac{\omega'\varepsilon_2(\omega')}{\omega'^2-\omega^2}d\omega' \quad (2)$$

With the knowledge of the complex dielectric tensor components all other frequency dependent optical constants can be obtained. Furthermore, the other optical parameters, such as absorption coefficient$I(\omega)$, refractive index $n(\omega)$ and energy-loss function$L(\omega)$, are derived from $\varepsilon_1(\omega)$ and $\varepsilon_2(\omega)$46. The investigated crystals have monoclinic symmetry, which has five nonzero components of the second-order dielectric

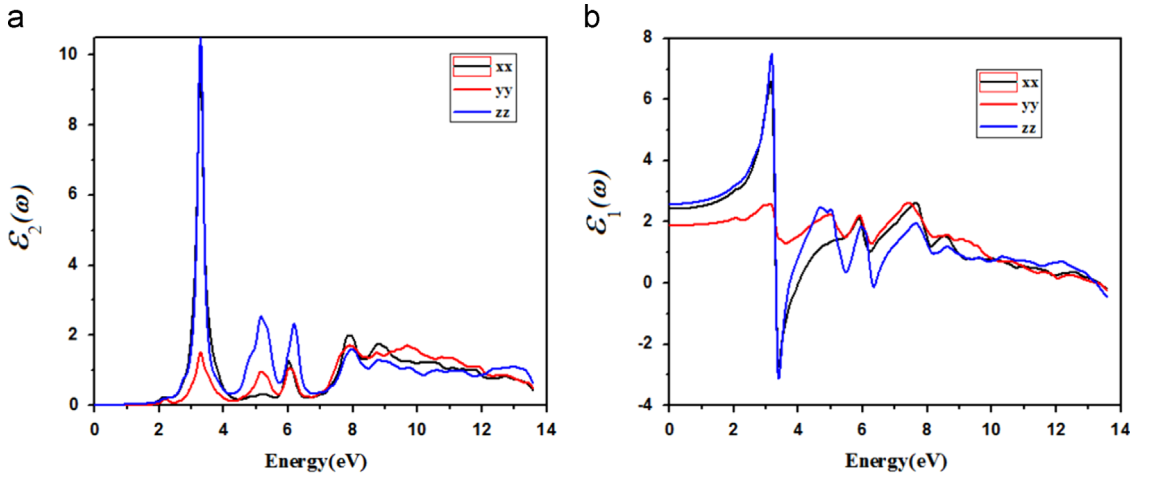

Fig. 5. Calculated imaginary $\varepsilon_2(\omega)$ and real part $\varepsilon_1(\omega)$ of dielectric tensor.

tensor. Regardless of this only $\varepsilon_2^{xx}(\omega)$, $\varepsilon_2^{yy}(\omega)$ and $\varepsilon_2^{zz}(\omega)$ are major, these are the imaginary parts of the frequency-dependent dielectric function. These components correspond to an electric field perpendicular and parallel to the *c*-axis. The calculated imaginary part for the investigated compound has been shown in Fig. 5a. The half-width broadening is taken to be 0.1 eV which is typical of the experimental accuracy. It is clear that there is a considerable anisotropy between the three spectra corresponding to different polarizations. The critical points (thresholds) for $\varepsilon_2^{xx}(\omega)$, $\varepsilon_2^{yy}(\omega)$ and $\varepsilon_2^{zz}(\omega)$ occur at 2.01 eV. The $\varepsilon_2^{xx}(\omega)$ and $\varepsilon_2^{yy}(\omega)$ components have their maximum values around 3.2 eV, and $\varepsilon_2^{zz}(\omega)$ at 8.0 eV. We should emphasize that the first peaks are mainly due to transitions from I-p orbital in the valence bands to N-p orbital in the conduction bands. Apart from the main peaks, the next peaks arise mainly from direct transitions between Cl-p and N-s orbital to Cl-s and I-p orbital. The weakness of the structures B and C compared to A (Fig. 5a) could be explained by the fact that $\varepsilon_2(\omega)$scales as $1/\omega^2$.

Table 4
Polarization directions.

	$\varepsilon_{xx}(\omega)$	$\varepsilon_{yy}(\omega)$	$\varepsilon_{zz}(\omega)$
$\varepsilon_1(0)$	2.40	1.8	2.56
$n_1(0)$	1.55	1.37	1.61

The results for the dispersive part of the dielectric function $\varepsilon_1(\omega)$ are shown in Fig. 5b. At high frequencies the zero crossing of$\varepsilon_1(\omega)$, which corresponds to the location of the screened plasma frequency is located at 3.29, 13.36 and 3.29 eV for $\varepsilon_1^{xx}(\omega)$, $\varepsilon_1^{yy}(\omega)$ and $\varepsilon_1^{zz}(\omega)$ respectively. The static dielectric constant $\varepsilon_1(0)$ is given by the low energy limit of $\varepsilon_1(\omega)$. It is necessary to emphasize that we do not include phonon contributions to the dielectric screening, and $\varepsilon_1(0)$ corresponds to the static optical dielectric constant. The obtained $\varepsilon_1(0)$ using EV-GGA formalism, along the crystal axes resolved into the three components are listed in Table 4. The calculated absorption coefficient, refractive index, electron energy-loss and reflectivity spectra are shown in Fig. 6a–d.

The absorption $I(\omega)$ coefficient spectra (Fig. 6a) rise steeply at the absorption edge to form the first highest peaks (highest absorption) at around 3.4 eV for all polarization directions. The absorption coefficient confirms the considerable anisotropy between the three polarizations.

The refractive indices $n(\omega)$ are closely related to the electronic polarizability of ions and the local field inside

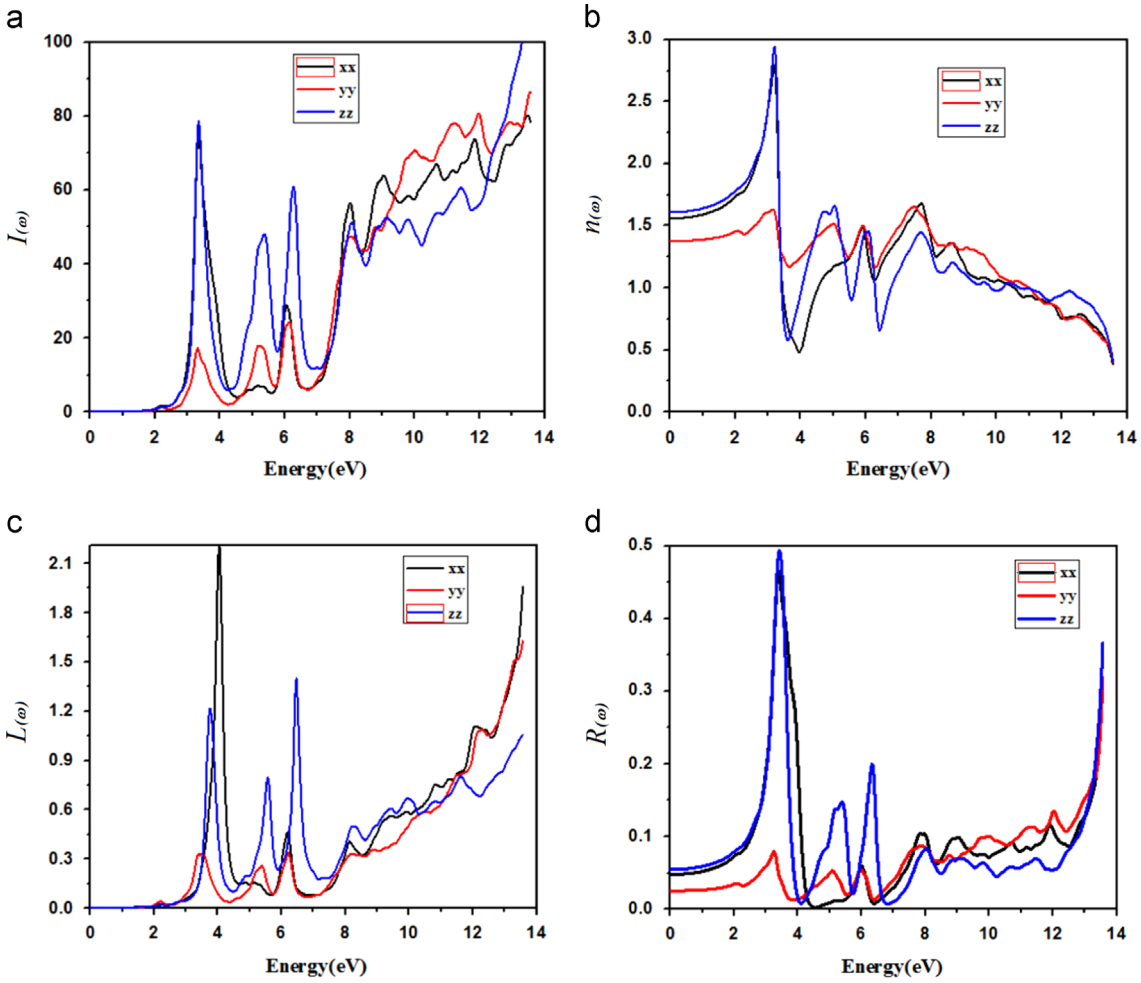

Fig. 6. Calculated absorption coefficient, energy-loss spectrum $L(\omega)$, and the refractive index $n(\omega)$.

the crystal. In Fig. 6b, we show the refractive indices of Di-2-pyrymidonium dichloride-di-iodide, a maximum can be observed in the spectrum between 2.0 and 3.5 eV, followed by a valley situated between 3.5 and 4.0 eV. Small humps are located in the energy region between 5.0 and 10.0 eV. At the higher energies the tail of the spectrum vanishes. The reason for vanishing of the curves at higher energy is due to the fact that beyond certain energy the material can no longer act as transparent material and it absorbs high energy photons. Our calculated $n(0)$ resolved into three polarization directions is given in Table 4. It is also clear from Fig. 6b that the refractive index falls below unity at a number of frequencies. Refractive index lesser than unity shows that the phase velocity of light is greater than the light celerity c, which might seem to imply a contradiction to relativity. However, this over looks the fact that a signal must be transmitted as a wave packet rather than monochromatic wave. In a dispersive medium, a wave packet will propagate at the group velocity v_g given by $v_g = dw/dk$ rather than at phase velocity $v = w/k = c/n$ where the relation between v_g and v is given by

$$v_g = v\left(1 - \frac{k\,dn}{n\,dk}\right) \tag{3}$$

This equation shows that v_g is always less than v. If we try to transmit a signal in a spectral region, where v is greater than c, we would always find that v_g is less than c.

The energy-loss spectrum is related to the energy loss of a fast electron traversing in the material and is usually large at the plasma energy. The plasmon losses correspond to a collective oscillation of the valence electrons and their energies are related to the density of valence electrons. In the case of inter-band transitions, which consist mostly of plasmon excitations, the scattering probability for volume losses is directly connected to the energy loss function. The frequency corresponding to the plasma resonance can be calculated from the energy loss spectrum shown in Fig. 6c. The most prominent peak in the energy-loss spectrum is identified as the plasmon peak and located at 4.0 eV for$\varepsilon_{xx}(\omega)$ polarization. The peaks in each of these spectra correspond to the peaks observed in the imaginary part $\varepsilon_2(\omega)$ of dielectric function.

The spectrum for the optical reflectivity$R(\omega)$is shown in Fig. 6d. The spectra shows the higher value (i.e. 50%) of $R(\omega)$ in the visible energy range of the investigated material in this range. The highest peak of $R(\omega)$ is located at energy 2.5–4.2 eV (50%); also $R(\omega)$ has a peak close to maximum with a value of 40% at 13.6 eV which is located in the UV region. Therefore, the investigated compound can be used as a shielding material from visible and UV radiations. The maximum reflectivity takes place where the real part of dielectric function $\varepsilon_1(\omega)$ becomes negative.

4. Conclusion

In summary, the electronic structures, electronic charge density and optical properties of Di-2-pyrymidonium dichloride-di-iodide were performed by means of the density functional theory within LDA and EVGGA. Di-2-pyrymidonium dichloride-di-iodide presented band gap value using EVGGA (2.01 eV) which is larger than that obtained within LDA (1.781 eV). The electronic charge density is also discussed in the $(-1\ 0\ 1)$ plane. The contour plot shows partial ionic and strong covalent bonding between C–O, N–C and C–H atoms. The dielectric optical properties were also calculated and discussed in detail. The real and imaginary parts of dielectric function and hence the optical constants such as energy loss and refractive index are calculated. From the study of reflectivity we deduced that the investigated compound can be used as a shielding material from visible and UV radiations. At present, there are no experimental results on the optical properties for the monoclinic Di-2-pyrymidonium dichloride-di-iodide as of yet. Therefore, we hope that our calculated results could serve as a reference for future study about the optical properties of Di-2-pyrymidonium dichloride-di-iodide.

Acknowledgment

The result was developed within the CENTEM project, Reg. no. CZ.1.05/2.1.00/03.0088, co-funded by the ERDF as a part of the Ministry of Education, Youth and Sports OP RDI program. Computational resources were provided by MetaCentrum (LM2010005) and CERIT-SC (CZ.1.05/3.2.00/08.0144) infrastructures.

References

[1] I.V. Kityk, J. Ulanski, J.K. Jeszka, A. Tracz, Adv. Mater. Opt. Electron. 6 (1996) 358–362.
[2] P.H. Svensson, L. Kloo, Chem. Rev. 103 (5) (2003) 1649–1684.
[3] P.D. Boyle, S.M. Godfrey, Coord. Chem. Rev. 223 (1) (2001) 265–299.
[4] P. Deplano, J.R. Ferraro, M.L. Mercuri, E.F. Trogu, Coord. Chem. Rev. 188 (1) (1999) 71–95.
[5] M.C. Aragoni, M. Arca, F.A. Devillanova, et al., Coord. Chem. Rev. 184 (1) (1999) 271–290.
[6] Ioanna-EfpraxiaParigoridi, et al., Dalton Trans. (2008) 5159–5165.
[7] J. Barluenga, F. Gonzalez-Bobes, M.C. Murguia, S.R. Ananthoju, J.M. Gonzalez, Chem.: Eur. J. 10 (2004) 4206–4213.
[8] D.B. Dess, J.C. Martin, J. Am. Chem. Soc. 113 (1991) 7277–7287.
[9] H. Tohma, S. Takizawa, T. Maegawa, Y. Kita, Angew. Chem. 112 (2000) 1362–1364.H. Tohma, S. Takizawa, T. Maegawa, Y. Kita, Angew. Chem. Int. Ed. 39 (2000) 1306–1308.
[10] S. Hanessian, D.H.-c. Wong, M. Therien, Synthesis (1981) 394–396.
[11] T.R. Beebe, F.M. Howard, J. Am. Chem. Soc. 91 (1969) 3379–3380.
[12] P. Blaha, K. Schwarz, G.K.H. Madsen, D. Kvasnicka, J. Luitz, WIEN2k: An Augmented Plane Wave Local Orbitals Program for Calculating Crystal Properties, Karlheinz Schwarz/Technical Universität Wien, Wien, 2001.
[13] K.M. Wong, S.M. Alay-e-Abbas, A. Shaukat, Y. Fang, Y. Lei, J. Appl. Phys. 113 (2013) 014304.
[14] K.M. Wong, S.M. Alay-e-Abbas, A. Shaukat, Y. Fang, Y. Lei, J. Appl. Phys. 114 (2013) 034901.
[15] J.P. Perdew, A. Zunger, Phys. Rev. B 23 (1981) 5048.
[16] E. Engel, S.H. Vosko, Phys. Rev. B 50 (1994) 10498.
[17] A.H. Reshak, S. Azam, J. Magn. Magn. Mater. 352 (2014) 72–80.
[18] A.H. Reshaka, B. WilayatKhan, J. Alloy. Compd. 591 (2014))362–369.
[19] S.A. Khan, A.H. Reshak, Int. J. Electrochem. Sci. 8 (2013) 9459–9473.
[20] A.H. Reshak, S.A. Khan, S. Auluck, RSC Adv. 4 (2014) 6957–6964.
[21] A.H. Reshak, S.A. Khan, Mater. Res. Bull. 48 (2013) 4555–4564.
[22] A.H. Reshak, S.A. Khan, J. Alloy. Compd. 595 (2014) 125–130.
[23] A.H. Reshak, S. Azam, J. Magn. Magn. Mater. 362 (2014) 204–215.
[24] A.H. Reshak, et al., J. Magn. Magn. Mater. 363 (2014) 133–139.
[25] A.H. Reshak, S. Azam, J. Magn. Magn. Mater. 358–359 (2014) 16–22.
[26] A.H. Reshak, S. Azam, J. Magn. Magn. Mater. 351 (2014) 98–103.
[27] A.H. Reshak, S. Azam, Int. J. Electrochem. Sci. 8 (2013) 10359–10375.
[28] A.H. Reshak, S. Azam, J. Magn. Magn. Mater. 352 (2014) 72–80.
[29] S. Azam, A.H. Reshak, Physica B431 (2013))102–108.
[30] S. Azam, A.H. Reshak, J. Organomet. Chem. 766 (2014) 22–33.
[31] S. Azam, A.H. Reshak, Solid State Sci. 32 (2014) 26–34.
[32] S. Azam, A.H. Reshak, RSC Adv. 4 (2014) 20102–20113.
[33] S. Azam, A.H. Reshak, Mater. Sci. Semicond. Process. 26 (2014) 649–656.